THE JOURNAL OF BIOLOGICAL CHEMISTRY VOL. 287, NO. 3, pp. 2191–2202, January 13, 2012

Inhibition of Phosphorylation of Na^+,K^+-ATPase by Mutations Causing Familial Hemiplegic Migraine*[S]

Received for publication, November 10, 2011, and in revised form, November 21, 2011 Published, JBC Papers in Press, November 23, 2011, DOI 10.1074/jbc.M111.323022

Vivien Rodacker Schack, Rikke Holm, and Bente Vilsen[1]

From the Department of Biomedicine, Aarhus University, DK-8000 Aarhus C, Denmark

Background: Familial hemiplegic migraine type II (FHM2) is caused by mutations in the Na^+,K^+-ATPase α2-isoform.
Results: Several FHM2 mutations inhibit phosphorylation or dephosphorylation.
Conclusion: These mutations cause FHM2 by local and long range effects on the catalytic site and not by reducing the affinity for external K^+.
Significance: Insights into the pathophysiological mechanism of FHM2 and the molecular mechanism of the Na^+,K^+-ATPase have been obtained.

The neurological disorder familial hemiplegic migraine type II (FHM2) is caused by mutations in the α2-isoform of the Na^+,K^+-ATPase. We have studied the partial reaction steps of the Na^+,K^+-pump cycle in nine FHM2 mutants retaining overall activity at a level still compatible with cell growth. Although it is believed that the pathophysiology of FHM2 results from reduced extracellular K^+ clearance and/or changes in Na^+ gradient-dependent transport processes in neuroglia, a reduced affinity for K^+ or Na^+ is not a general finding with the FHM2 mutants. Six of the FHM2 mutations markedly affect the maximal rate of phosphorylation from ATP leading to inhibition by intracellular K^+, thereby likely compromising pump function under physiological conditions. In mutants R593W, V628M, and M731T, the defective phosphorylation is caused by local perturbations within the Rossmann fold, possibly interfering with the bending of the P-domain during phosphoryl transfer. In mutants V138A, T345A, and R834Q, long range effects reaching from as far away as the M2 transmembrane helix perturb the function of the catalytic site. Mutant E700K exhibits a reduced rate of E_2P dephosphorylation without effect on phosphorylation from ATP. An extremely reduced vanadate affinity of this mutant indicates that the slow dephosphorylation reflects a destabilization of the phosphoryl transition state. This seems to be caused by insertion of the lysine between two other positively charged residues of the Rossmann fold. In mutants R202Q and T263M, effects on the A-domain structure are responsible for a reduced rate of the E_1P to E_2P transition.

Hemiplegic migraine is a severe subtype of migraine with aura associated with transient motor weakness and sensory as well as speech difficulties. It is autosomal dominantly inherited (familial hemiplegic migraine). Besides mutations in neuronal voltage-gated Ca^{2+} and Na^+ channels (FHM1 and FHM3), familial hemiplegic migraine has been associated with mutations in the α2-isoform of the Na^+,K^+-ATPase (FHM2) (1). The Na^+ and K^+ gradients created across the cell membrane by the Na^+,K^+-ATPase are of vital importance for cellular function and activities, including generation of action potentials and secondary active transport of ions, nutrients, and neurotransmitters. In the mammalian brain, three different isoforms of the catalytic α-subunit are expressed, α1, α2, and α3. The α2-isoform is mainly distributed in glial cells, whereas the α3-isoform is found in neurons and is absent in glial cells (2). So far, we know of more than 50 Na^+,K^+-ATPase α2 mutations associated with hemiplegic migraine. It has been suggested that the pathophysiology results from an impaired clearance of extracellular K^+, producing a wide cortical depolarization (3, 4). Moreover, the gradients of both Na^+ and K^+ are important for the reuptake of the excitatory transmitter glutamate from the synaptic cleft via the glutamate transporter, and impaired Na^+ transport would also lead to a rise of intracellular Ca^{2+} via the Na^+/Ca^{2+} exchanger with secondary effects on Ca^{2+} signaling (1, 5, 6). Cell survival studies of transfected cells, in which the wild type has been inhibited by ouabain, have demonstrated the inability of certain FHM2 mutants to sustain cell growth in accordance with the theory of haploinsufficiency, *i.e.* only the wild type allele encodes a functional enzyme (1, 7). Other FHM2 mutants have nevertheless been found to retain transport function (4, 8–11), and more functional mutants exist, as indicated by the present results. A crucial question is therefore whether and how their function deviates from that of the wild type. One study has reported a 2-fold reduced apparent K^+ affinity for activation of the ATPase reaction of mutant T345A, which was suggested to give rise to a reduced rate of external K^+ clearance *in vivo* (4).

To fully understand the functional implications of the FHM2 mutations and the structural basis, it is necessary to reveal the mutational effects on the individual partial reaction steps of the pump cycle and the interaction with Na^+ and K^+ and to try to relate the observed effects to known structural features. We present here the functional consequences of nine Na^+,K^+-ATPase α2 mutations, including T345A, which all have been found in patients exhibiting the characteristic symptoms of hemiplegic migraine (12–17). The α-subunit carrying the

* This work was supported in part by grants from the Danish Medical Research Council, the Novo Nordisk Foundation (Fabrikant Vilhelm Pedersen og Hustrus Legat), and the Lundbeck Foundation.
[S] This article contains supplemental Table S1.
[1] To whom correspondence should be addressed: Dept. of Biomedicine, Aarhus University, Ole Worms Allé 6, Bldg. 1180, DK-8000 Aarhus C, Denmark. E-mail: bv@fi.au.dk.

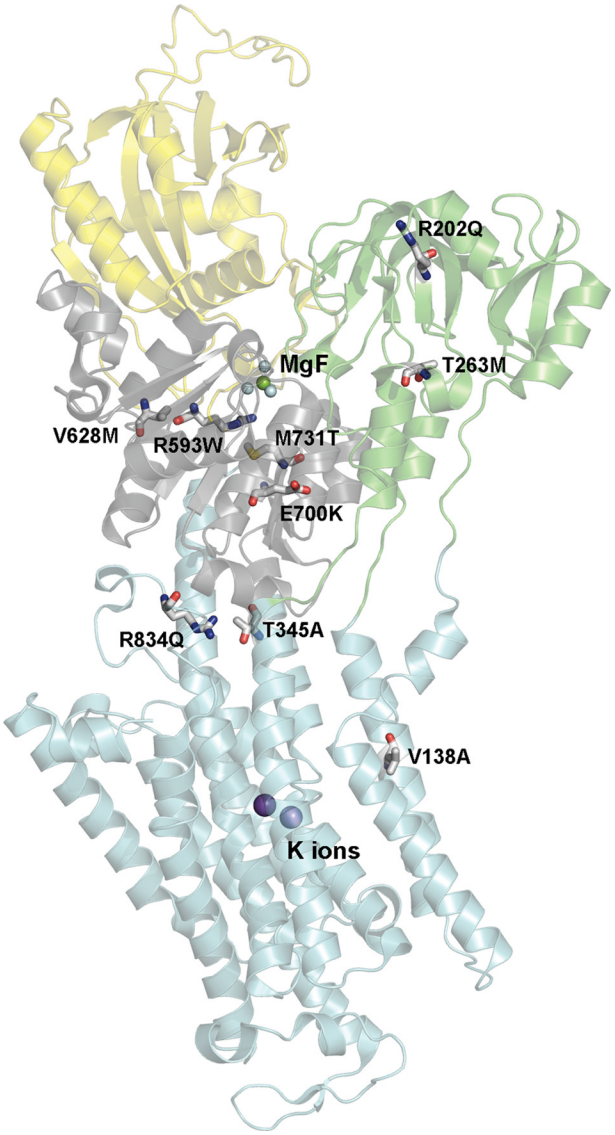

FIGURE 1. **Na^+,K^+-ATPase structure with indication of the FHM2 mutations studied.** The structure shown has Protein Data Bank code 2ZXE ($E_2[K_2]$ with bound MgF_4^{2-} as phosphate analog (19)). Color codes for P-, A-, N-, and M-domain are *gray, green, yellow,* and *cyan*, respectively. The bound K^+ ions are shown as *purple spheres* and MgF_4^{2-} (*MgF*) in the catalytic site as one *green sphere* with *four cyan spheres*. The mutated residues (numbered according to the human α2-isoform) are highlighted as *sticks* colored according to the elements (carbon, *gray*; oxygen, *red*; nitrogen, *blue*; sulfur, *yellow*).

mutations consists of 10 transmembrane helices M1–M10 (harboring the Na^+- and K^+-binding sites) and a cytoplasmic "head" made up of three subdomains as follows: A ("actuator"), N ("nucleotide binding"), and P ("phosphorylation") (18, 19). Generally, FHM2 mutations are widely scattered over the Na^+,K^+-ATPase protein, but with a preference for the P-domain (7). Four of the mutations investigated here are located in the P-domain (R593W, V628M, E700K, and M731T), two are in the A-domain (R202Q and T263M), one is in M2 (V138A), another is in M4 near the interface to the P-domain (T345A), and the last is in the L6–7 loop between M6 and M7 close to the P-domain (R834Q) (Fig. 1). We assessed their functional impact in a panel of analyses of the partial reaction steps (*cf.* Scheme 1), using both steady-state and transient kinetic measurements, the latter allowing determination of the rates of the

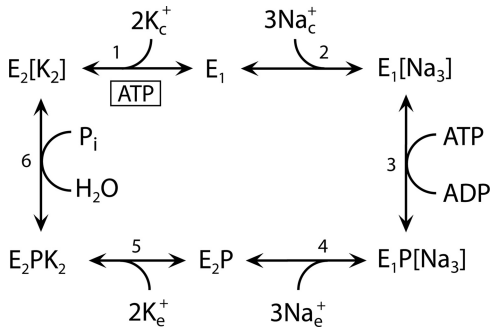

SCHEME 1. **Model of the reaction cycle of Na^+,K^+-ATPase ("Post-Albers scheme").** Ligand binding and dissociation steps and conformational changes between E_1/E_1P and E_2/E_2P forms are indicated. Na^+ binds from the cytoplasmic side to the E_1 form and activates phosphorylation from ATP bound with high affinity to E_1. The E_1P form is ADP-sensitive, *i.e.* able to donate the phosphoryl group back to ADP, forming ATP. The E_2P form is K^+-sensitive, *i.e.* hydrolysis of E_2P is activated by binding of K^+ from the extracellular side. Occluded ions are shown in *brackets*. Subscripts *c* and *e* indicate the cytoplasmic and extracellular sides, respectively. The ATP molecule binding with low affinity to E_2 is shown *boxed*. Because ATP binds with higher affinity to E_1 than to E_2, an increase in the apparent affinity for ATP upon mutation reflects a shift of the E_1-E_2 distribution toward the E_1 form, whereas a decrease in the affinity for ATP reflects a shift toward the E_2 form.

rapid phosphorylation and dephosphorylation reactions. The observed effects are analyzed in the context of information derived from the recently determined crystal structures of the Na^+,K^+-ATPase (18, 19).

EXPERIMENTAL PROCEDURES

FHM2 mutations were introduced into full-length cDNA encoding an ouabain-resistant version of the human α2-isoform (4). Mutants and wild type were expressed in COS-1 cells under ouabain selection pressure (20). The plasma membrane fraction was isolated and made leaky to allow access of incubation media from both sides of the membrane, and Na^+,K^+-ATPase activity was studied at 37 °C by following the liberation of P_i (20). The catalytic turnover rate was calculated by relating the ATPase activity to the active site concentration determined by phosphorylation at 0 °C in the presence of 150 mM Na^+ and oligomycin (21, 22). Measurements of phosphorylation and dephosphorylation were performed using either a manual mixing technique at 0 °C or a QFM-5 quench-flow module (Bio-Logic Instruments, Claix, France), allowing transient kinetic studies at 25 °C (21, 22). To eliminate the contribution of the endogenous Na^+,K^+-ATPase, ouabain was included in the reaction media (21). Data processing was performed using SigmaPlot (SPSS, Inc.) for linear regression analysis (21), and the results are reported as average values ± S.E. (shown by *error bars* in figures when larger than the size of the symbols). The number of independent determinations is indicated by *n* in Tables 1 and 2. Structural figures were prepared using PyMOL.

RESULTS

Overall Function—The nine FHM2 mutations were introduced into the ouabain-resistant version of the human α2-isoform, and the mutants were expressed in mammalian COS-1 cells and subjected to ouabain-selection pressure (20), taking advantage of the >100-fold difference between the ouabain affinities of the exogenous Na^+,K^+-ATPase and the endogenous COS cell enzyme. Like the wild type, all mutants were able

TABLE 1
ATPase activity parameters

	Ouabain-affinity[a]	Turnover rate[b]	$K_{0.5}(K^+)$[c]	$K_{0.5}(VO_4^{3-})$[c]	$K_{0.5}$(ATP)[c]
	μM	min^{-1}	μM	μM	μM
Wild type α2	297 ± 29 (n = 3)	6843 ± 380 (n = 6)	716 ± 19 (n = 5)	27 ± 2 (n = 6)	104 ± 6 (n = 8)
V138A	693 ± 38 (n = 3)	3768 ± 157 (n = 6)	763 ± 18 (n = 4)	290 ± 18 (n = 4)	47 ± 2 (n = 7)
R202Q	288 ± 40 (n = 3)	5420 ± 277 (n = 10)	748 ± 33 (n = 5)	113 ± 6 (n = 8)	67 ± 4 (n = 4)
T263M	1323 ± 95 (n = 3)	3233 ± 168 (n = 6)	465 ± 19 (n = 5)	73 ± 4 (n = 8)	21 ± 1 (n = 4)
T345A	657 ± 48 (n = 4)	3419 ± 50 (n = 6)	747 ± 20 (n = 4)	283 ± 21 (n = 5)	31 ± 2 (n = 5)
R593W	2409 ± 518 (n = 4)	1029 ± 56 (n = 6)	263 ± 35 (n = 7)	>1000 (n = 6)	19 ± 1 (n = 6)
V628M	1282 ± 206 (n = 3)	1885 ± 63 (n = 6)	273 ± 15 (n = 4)	>1000 (n = 5)	71 ± 6 (n = 5)
E700K	146 ± 23 (n = 3)	3669 ± 229 (n = 7)	1145 ± 36 (n = 3)	>1000 (n = 6)	28 ± 1 (n = 3)
M731T	2708 ± 597 (n = 3)	1238 ± 84 (n = 6)	216 ± 9 (n = 5)	778 ± 14 (n = 3)	26 ± 1 (n = 3)
R834Q	2134 ± 534 (n = 3)	1236 ± 46 (n = 6)	332 ± 21 (n = 5)	>1000 (n = 4)	24 ± 2 (n = 5)

[a] The rate of ATP hydrolysis was determined at 37 °C in the presence of 130 mM NaCl, 20 mM KCl, 3 mM ATP, 3 mM $MgCl_2$, 30 mM histidine buffer (pH 7.4), 1 mM EGTA, and various concentrations of ouabain. The data points were fitted using a function with the ouabain-inhibited enzyme represented by the sum of two hyperbolic components corresponding to the exogenous enzyme (affinity constant K_1) and the endogenous COS cell enzyme (affinity constant $K_2 \leq 1$ μM), respectively (24): $V/V_{max} = 1 - a_1[\text{ouabain}]/(K_1 + [\text{ouabain}]) - a_2[\text{ouabain}]/(K_2 + [\text{ouabain}])$. The values determined for K_1 are indicated in the table.

[b] The Na^+,K^+-ATPase activity was determined at 37 °C in the presence of 30 mM histidine buffer (pH 7.4), 130 mM NaCl, 3 mM ATP, 3 mM $MgCl_2$, 1 mM EGTA, ouabain to inhibit the endogenous enzyme, and 20 mM KCl. The catalytic turnover rate was calculated as the ratio between the Na^+,K^+-ATPase activity and the active site concentration (maximum phosphorylation from [γ-^{32}P]ATP measured at 0 °C in the presence of 150 mM NaCl and oligomycin) (21, 22).

[c] $K_{0.5}$ values for K^+ activation, vanadate inhibition, and ATP activation were extracted from the data in Figs. 2, 8 and 9, respectively.

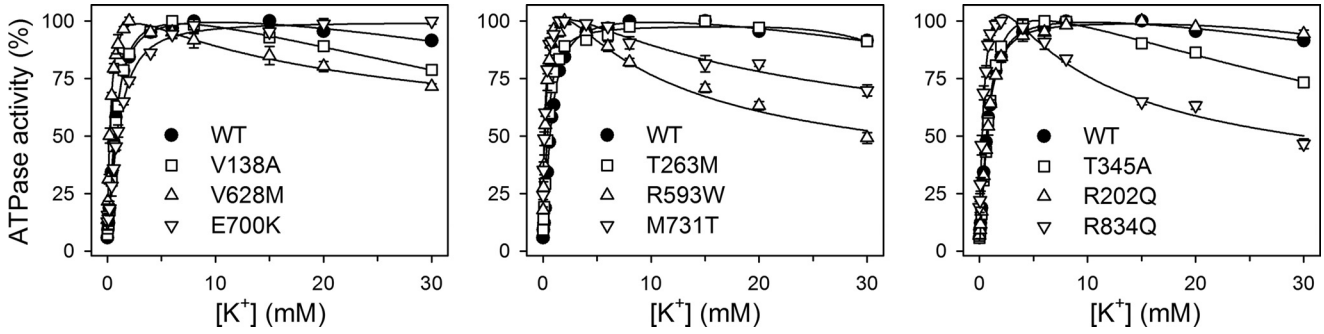

FIGURE 2. **K^+ dependence of Na^+,K^+-ATPase activity.** ATPase activity was measured at 37 °C in 40 mM NaCl, 3 mM ATP, 3 mM $MgCl_2$, 30 mM histidine (pH 7.4), 1 mM EGTA, 10 μM ouabain, and K^+ concentrations as indicated. $K_{0.5}$ values for K^+ activation are listed in Table 1.

to confer ouabain resistance in growth medium containing 5 μM ouabain, indicating that the rate of transport of Na^+ and K^+ is sufficiently high to sustain cell growth. Determination of the ouabain dependence of Na^+,K^+-ATPase activity showed 2–9-fold reduction of the apparent affinity for ouabain for mutants V138A, T263M, T345A, R593W, V628M, M731T, and R834Q, wild type-like apparent affinity for R202Q, and 2-fold increased apparent affinity for E700K (Table 1). Hence, all the functional studies described below were carried out in the presence of ouabain to selectively inhibit the endogenous Na^+,K^+-ATPase ($K_{0.5} \leq 1$ μM).

The catalytic turnover rate determined in the presence of 130 mM Na^+, 20 mM K^+, and a saturating concentration of MgATP was found reduced in all mutants, most severely for R593W, V628M, M731T, and R834Q, displaying less than one-third the turnover rate of the wild type. T263M, T345A, E700K, and V138A displayed a turnover rate around 50%, whereas R202Q showed ~20% reduction (Table 1).

K^+ Interaction—A critical issue is whether the affinity for external K^+ is lowered, thereby resulting in reduced ability to clear K^+ from the extracellular space. The interaction with K^+ was investigated by determining the K^+ dependence of ATPase activity (Fig. 2). In the wild type, K^+ at a submillimolar concentration activates ATP hydrolysis by binding at extracellularly facing sites of the E_2P form, thereby stimulating dephosphorylation (*cf.* Scheme 1, *Reaction 6*). The majority of the mutants displayed a $K_{0.5}$ value for K^+ activation similar to or lower (*i.e.* corresponding to higher affinity) than that determined for the wild type, with E700K being the only exception, exhibiting a slight 1.6-fold increase in the $K_{0.5}$ value for K^+ activation relative to wild type (Fig. 2 and Table 1). K^+ concentrations above 15 mM inhibited the wild type somewhat, which is explained by K^+ binding in competition with Na^+ at the cytoplasmically facing sites of the enzyme in E_1 conformation, leading to conversion of E_1 back to the K^+-occluded E_2 state (*cf.* Scheme 1, *Reaction 1*) (23, 24). Mutants V138A, T345A, R593W, V628M, M731T, and R834Q exhibited a more distinct inhibitory phase than the wild type, whereas no inhibition was observed for E700K at the K^+ concentrations studied (Fig. 2).

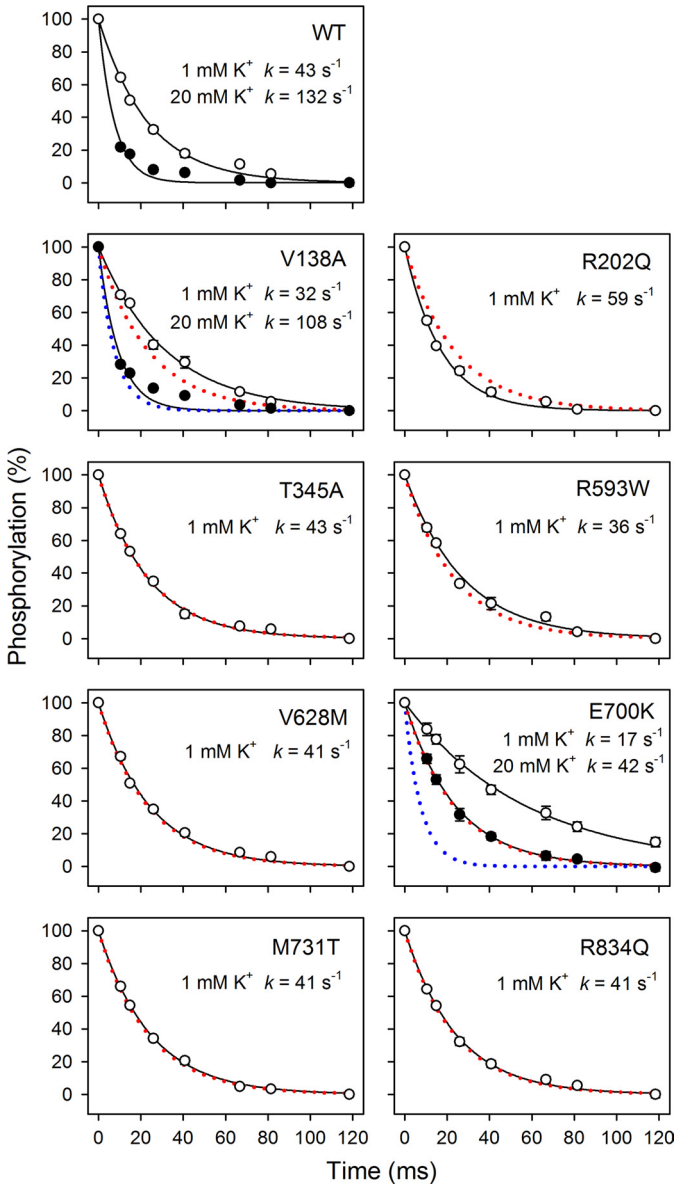

FIGURE 3. **Rapid kinetic measurements of K^+-induced E_2P dephosphorylation.** Phosphorylation was performed for 5 s at 25 °C in the presence of 2 μM [γ-^{32}P]ATP in 20 mM Tris (pH 7.5), 20 mM NaCl, 3 mM $MgCl_2$, 1 mM EGTA, 130 mM choline chloride, and 10 μM ouabain, followed by dephosphorylation for the indicated times in the same medium containing in addition 1 mM nonradioactive ATP and 1 mM K^+ (*open symbols*) or 20 mM K^+ (*filled symbols*). Each *line* represents the best fit of a mono-exponential decay function, giving the indicated rate constants (also listed in Table 2 with statistics). The wild type data are represented in each panel by *dotted red* and *blue lines*.

Because the variable inhibitory phase in the K^+ dependence of ATPase activity inevitably will influence the apparent affinity for K^+ activation corresponding to the rising phase, the activation by extracellular K^+ was also examined more directly by determining the rate of E_2P dephosphorylation (Fig. 3 and Table 2). At a nonsaturating K^+ concentration of 1 mM (Fig. 3, *open symbols*), T345A, R593W, V628M, M731T, and R834Q displayed a dephosphorylation rate constant almost identical to that of the wild type, indicating that these mutations did not weaken the interaction with extracellular K^+. R202Q exhibited a higher rate constant of dephosphorylation than wild type. By contrast, the dephosphorylation rate constant was reduced for V138A and E700K relative to wild type (1.3- and 2.5-fold, respectively). To determine whether this was related to a reduction in affinity for external K^+, similar experiments were performed at a saturating K^+ concentration of 20 mM (Fig. 3, *filled symbols*). The calculated ratios between the dephosphorylation rate constants at 1 and 20 mM K^+ are 0.29 ± 0.02, 0.42 ± 0.04, and 0.32 ± 0.02 for V138A, E700K, and wild type, respectively. Hence, at 1 mM K^+, the saturation of the external sites is similar to wild type for V138A and is actually higher for E700K, indicating that the reduced dephosphorylation rate is caused by a lower V_{max} of phosphoenzyme hydrolysis rather than a lower affinity for K^+.

Na^+ Interaction—Phosphorylation from ATP is triggered when three Na^+ ions have bound to intracellularly facing high affinity sites of the E_1 form and become occluded in the $E_1[Na_3]$ form (Scheme 1, *Reaction 2*) (25). To assess the Na^+ affinity of the E_1 form of the mutants, we studied the Na^+ dependence of phosphorylation from ATP in the absence of K^+ and presence of oligomycin to support occlusion (Fig. 4). The mutants displayed affinities similar to that obtained for the wild type; only R834Q exhibited a more than 2-fold reduced apparent affinity for Na^+ relative to wild type.

Rate of Phosphorylation—Because oligomycin stabilizes the Na^+-occluded $E_1[Na_3]$ form, thereby promoting phosphorylation (25, 26) and blocking the E_1P-E_2P transition (Scheme 1, *Reaction 4*), the presence of oligomycin enables the phosphoenzyme to build up a maximum level. Table 2 lists the level of phosphoenzyme accumulated at 150 mM NaCl in the absence of oligomycin relative to the maximum level obtained in the presence of oligomycin (EP/EP_{oligo}). Mutants R593W, V628M, M731T, and R834Q displayed a markedly reduced EP/EP_{oligo} ratio, and V138A and T345A showed a slight reduction relative to wild type, whereas T263M and E700K displayed higher EP/EP_{oligo} ratios than the wild type. Such effects can be due to changes in either the rate of phosphorylation or the rate of dephosphorylation. In the presence of oligomycin, the level of phosphoenzyme built up was sufficiently high to allow rapid kinetic studies of the rate of phosphorylation at a millisecond time scale at 25 °C, and thus the time course of phosphorylation in the presence of 2 μM ATP was determined (Fig. 5). Mutants V138A, T345A, R593W, V628M, M731T, and R834Q all displayed a reduced rate constant relative to wild type, most pronounced for M731T, suggesting that either the phosphorylation reaction or the binding of ATP is affected in these mutants. To determine the maximal rate of phosphorylation and the apparent affinity of these mutants for ATP we performed the analysis at varying ATP concentrations. E700K was included, because the dephosphorylation studies (Fig. 3) indicated that the catalytic site might be defective in this mutant. In Fig. 6, the results are depicted as double-reciprocal plots of the initial phosphorylation rate per ATPase molecule as a function of the concentration of ATP. The linear dependence allows extraction of the maximal phosphorylation rate per ATPase molecule, V_{max}, and the apparent affinity for ATP (the Michaelis constant K_m). M731T exhibited a most severe 6-fold reduction of V_{max}, relative to wild type. Mutants V138A, T345A, R593W, V628M, and R834Q showed 2–3-fold reduction, whereas E700K was wild type-like (Table 2). None of the mutations increased the

TABLE 2
Phosphorylation parameters

	$K_{0.5}(Na^+)$[a]	EP/EP_{oligo}[b]	k_{phos}, 2 μMATP[c]	V_{max}[c]	K_m[c]	E_1P[d]	Rate of E_2P dephosphorylation[e]	
							1 mM K^+	20 mM K^+
	μM	%	s^{-1}	s^{-1}	μM	%	s^{-1}	s^{-1}
Wild type α2	538 ± 15 (n = 8)	76 ± 2 (n = 5)	22 ± 1 (n = 3)	83 ± 10 (n = 8)	6.7 ± 0.8 (n = 8)	44 ± 4 (n = 9)	43 ± 2 (n = 6)	132 ± 5 (n = 3)
V138A	807 ± 25 (n = 4)	56 ± 3 (n = 6)	12 ± 1 (n = 5)	45 ± 8 (n = 13)	5.1 ± 1.0 (n = 13)	48 ± 9 (n = 5)	32 ± 2 (n = 3)	108 ± 4 (n = 3)
R202Q	541 ± 13 (n = 7)	76 ± 3 (n = 5)	17 ± 1 (n = 3)	ND	ND	61 ± 2 (n = 6)	59 ± 4 (n = 3)	ND[b]
T263M	633 ± 20 (n = 6)	85 ± 5 (n = 6)	23 ± 1 (n = 3)	ND	ND	96 ± 2 (n = 4)	ND[a]	ND[b]
T345A	814 ± 34 (n = 7)	59 ± 3 (n = 3)	13 ± 1 (n = 3)	39 ± 2 (n = 9)	4.5 ± 0.2 (n = 9)	33 ± 14 (n = 4)	43 ± 2 (n = 3)	ND[b]
R593W	694 ± 23 (n = 7)	16 ± 2 (n = 3)	10 ± 1 (n = 3)	28 ± 10 (n = 10)	5.1 ± 2.0 (n = 10)	71 ± 6 (n = 10)	36 ± 2 (n = 3)	ND[b]
V628M	890 ± 29 (n = 7)	18 ± 2 (n = 4)	12 ± 1 (n = 3)	45 ± 11 (n = 7)	5.9 ± 1.5 (n = 7)	74 ± 6 (n = 4)	41 ± 2 (n = 3)	ND[b]
E700K	621 ± 19 (n = 6)	85 ± 2 (n = 4)	20 ± 1 (n = 2)	69 ± 3 (n = 7)	5.3 ± 0.2 (n = 7)	59 ± 5 (n = 5)	17 ± 1 (n = 3)	42 ± 3 (n = 3)
M731T	218 ± 10 (n = 8)	30 ± 1 (n = 5)	5 ± 1 (n = 4)	14 ± 3 (n = 11)	3.0 ± 0.7 (n = 11)	66 ± 4 (n = 5)	41 ± 2 (n = 5)	ND[b]
R834Q	2496 ± 89 (n = 7)	21 ± 4 (n = 5)	15 ± 1 (n = 3)	35 ± 13 (n = 9)	5.9 ± 2.3 (n = 9)	56 ± 4 (n = 6)	41 ± 2 (n = 6)	ND[b]

[a] Extracted from the data in Fig. 4.
[b] Ratio between phosphorylation levels without (EP) and with oligomycin (EP_{oligo}). Phosphorylation was carried out for 10 s at 0 °C in 20 mM Tris (pH 7.5), 3 mM $MgCl_2$, 2 μM [γ-^{32}P]ATP, 10 μM ouabain, 150 mM NaCl, without and with 20 μg of oligomycin/ml.
[c] Extracted from the data in Figs. 5 and 6. The kinetic parameters were not determined (ND) for R202Q and T263M, because the phosphorylation rate at 2 μM ATP was close to wild type.
[d] Extracted from the data in Fig. 7.
[e] Extracted from the data in Fig. 3. For T263M, the E_2P dephosphorylation rate constant was not determined (ND), because the high extent of accumulation of E_1P, even at 25 °C, precluded such a determination. The dephosphorylation rate at 20 mM K^+ was determined only when the dephosphorylation at 1 mM K^+ was slower than that of the wild type.

K_m value. A significant reduction of K_m is noted for M731T (Fig. 6 and Table 2), likely reflecting the marked reduction of V_{max}, which leads to increased accumulation of nonphosphorylated enzyme with ATP bound. According to the equation $K_m = (k_{-1} + k_2)/k_1$, where k_1 and k_{-1} are the respective rate constants for binding and dissociation of ATP, and k_2 equals V_{max} (measured in units of rate per ATPase molecule), the K_m value will decrease with k_2, unless k_{-1} is much higher than the k_2 value, which is not the case here, because Na^+,K^+-ATPase binds the nucleotide rather tightly (27). In an analogous way, the accumulation of E_1 explains the increased apparent affinity for Na^+ in M731T (Table 2).

E_1P-E_2P Distribution—The phosphorylated form of the Na^+,K^+-ATPase exists in E_1P and E_2P states that can be distinguished by their different sensitivities to K^+ and ADP (Scheme 1). To estimate the extent of each phosphoenzyme pool present at steady state, the dephosphorylation time course was examined following addition of ADP to the phosphoenzyme. A biexponential function could be fitted to the data, permitting extraction of a rapid and a slow decay component, reflecting the initial amounts of E_1P and E_2P, respectively (Fig. 7). Table 2 lists the E_1P fraction. Notably, mutant T263M displayed a marked increase in the level of E_1P (to 96% *versus* 44% for the wild type). The other mutants displayed a less pronounced shift of the E_1P-E_2P distribution toward the E_1P form or were wild type-like.

Vanadate and ATP Affinities—Vanadate is an inhibitor that acts as analog of the phosphoryl group in the transition state during E_2P hydrolysis and binds exclusively to the enzyme in the E_2 conformation (28). The properties of the E_2 state were investigated by determining the apparent affinity for vanadate inhibition of ATP hydrolysis (Fig. 8). All the mutants exhibited a reduced apparent affinity for vanadate (Table 1). For R593W, V628M, E700K, M731T, and R834Q, the affinity was extremely low (≥30-fold reduced relative to wild type); in fact, no significant inhibition was seen for E700K within the vanadate concentration range examined (Fig. 8, *right panel*). A reduced sensitivity to vanadate inhibition can in principle arise from either a lowering of the intrinsic binding affinity of E_2 (possibly reflecting destabilization of the transition state of E_2P hydrolysis) or from a shift of the E_1-E_2 distribution away from the vanadate binding E_2 form in favor of E_1. To examine the mutational effects on the E_1-E_2 distribution, the ATP dependence of ATPase activity was also studied (Fig. 9). Because ATP binds with higher affinity to E_1 than to E_2, an increase in the apparent affinity for ATP upon mutation reflects a shift of the E_1-E_2 distribution toward the E_1 form, whereas a decrease in the affinity for ATP reflects a shift toward the E_2 form. The results summarized in Table 1 show a significant increase of the apparent ATP affinity for all the mutants (2–5-fold), indicating a shift toward the E_1 form. However, for R593W, V628M, E700K, M731T, and R834Q, the effect on ATP affinity was much less spectacular than the reduction of vanadate affinity, indicating that the latter arises not only from a shift in E_1-E_2 distribution but also from a change in the intrinsic affinity of the E_2 form for vanadate.

DISCUSSION

The nine FHM2 mutations studied here, which are found in various regions of the Na^+,K^+-ATPase α2-isoform, lead to a functionally altered but active enzyme capable of sustaining cell viability. Our results do not lend support to the hypothesis that

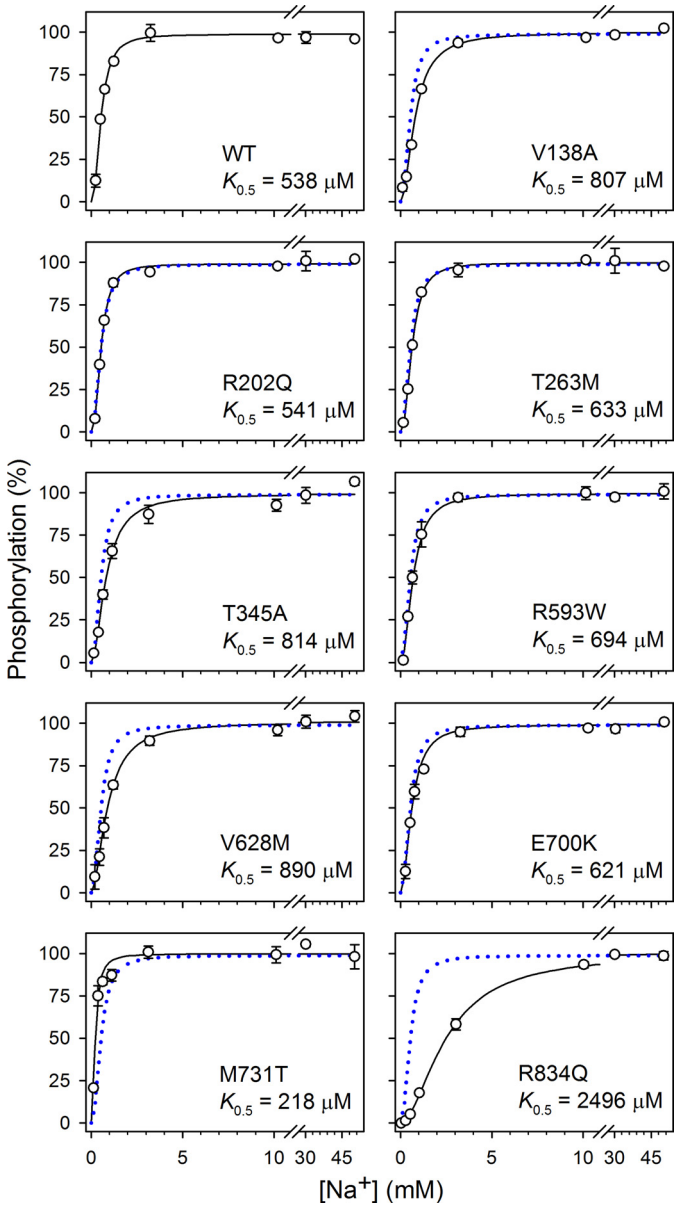

FIGURE 4. **Na^+ dependence of phosphorylation.** Phosphorylation was carried out for 10 s at 0 °C in 20 mM Tris (pH 7.5), 3 mM $MgCl_2$, 2 μM [γ-^{32}P]ATP, 10 μM ouabain, 20 μg of oligomycin/ml, NaCl to obtain the indicated concentrations of Na^+, and various concentrations of *N*-methyl-D-glucamine to maintain the ionic strength. Oligomycin was added to optimize phosphorylation and prevent dephosphorylation, thereby minimizing effects on apparent Na^+ affinity of variation of the phosphorylation and dephosphorylation rates. Each *line* represents the best fit of the equation $EP = EP_{max}\cdot[Na^+]^n/(K_{0.5}{}^n + [Na^+]^n)$, giving the indicated $K_{0.5}$ values (also listed in Table 2 with statistics). The data corresponding to wild type are represented in each panel by a *dotted blue line*.

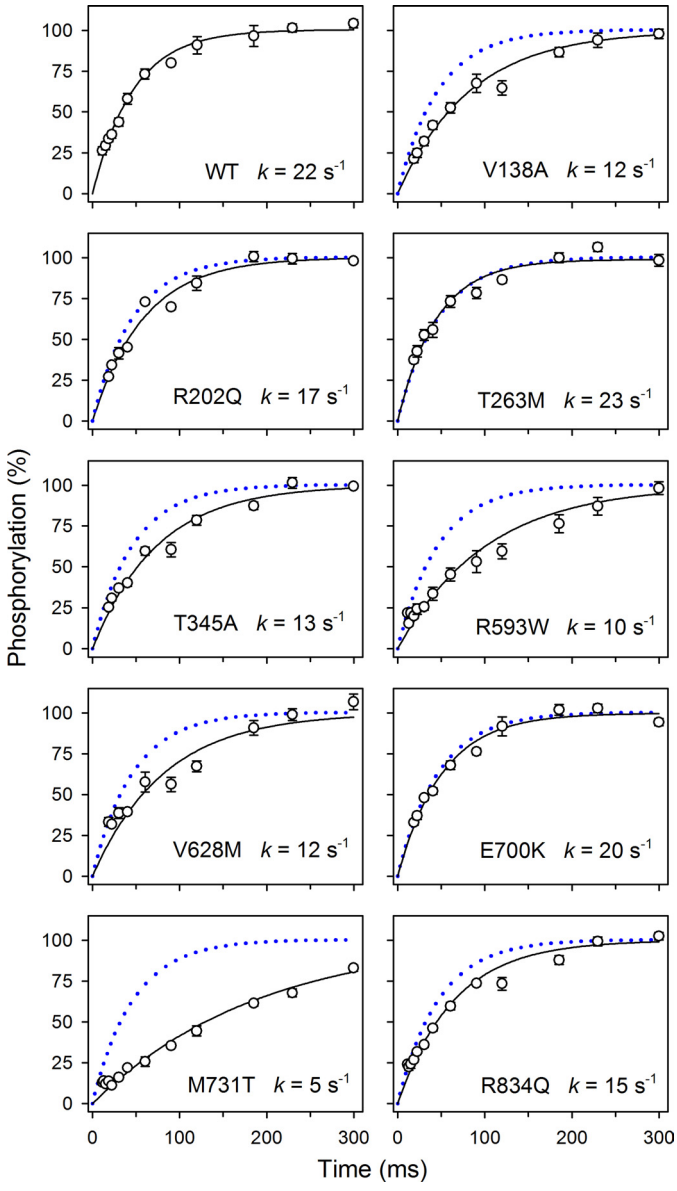

FIGURE 5. **Rapid kinetic measurements of phosphorylation rate.** Phosphorylation was performed for the indicated times at 25 °C in the presence of 2 μM [γ-^{32}P]ATP, 100 mM NaCl, 40 mM Tris (pH 7.5), 3 mM $MgCl_2$, 1 mM EGTA, 10 μM ouabain, and 20 μg/ml oligomycin. Each line represents the best fit of a mono-exponential "rise to max function," giving the indicated rate constants. The wild type data are represented in each panel by a *dotted blue line*.

a reduced affinity for external K^+, causing a selective disturbance of K^+ clearance, is an obligatory part of the mechanism underlying the disease (4). Neither can a defective Na^+ interaction generally account for the pathophysiology of the disease, as only R834Q exhibited a significant reduction of the Na^+ affinity. This is contrary to the neurological disorder rapid-onset dystonia parkinsonism, caused by mutation of the α3-isoform of Na^+,K^+-ATPase, where all mutants characterized so far display markedly reduced Na^+ affinity (21, 29, 30). At saturating Na^+ and K^+ concentrations, the FHM2 mutants studied here

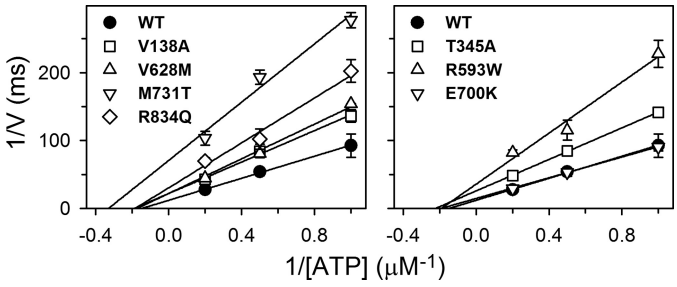

FIGURE 6. **ATP dependence of phosphorylation rate.** Initial rates of phosphorylation, determined as in Fig. 5 at 1, 2, and 5 μM [γ-^{32}P]ATP, are shown as a function of ATP concentration in double-reciprocal plots. For V_{max} and K_m values, see Table 2.

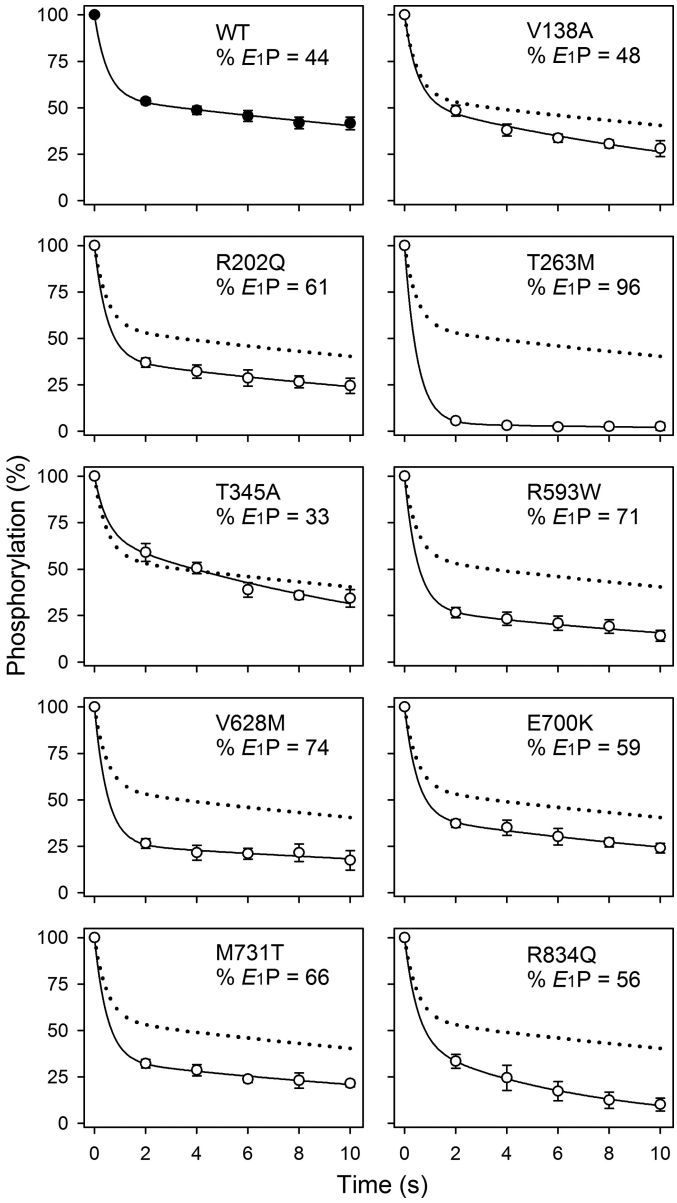

FIGURE 7. **Distribution of the phosphoenzyme between E_1P and E_2P.** Phosphorylation was carried out for 10 s at 0 °C in the presence of 2 μM [γ-^{32}P]ATP, 20 mM NaCl, 130 mM choline chloride, 20 mM Tris (pH 7.5), 3 mM $MgCl_2$, 1 mM EGTA, and 10 μM ouabain. Dephosphorylation was followed by addition of a chase solution producing final concentrations of 2.5 mM ADP and 1 mM unlabeled ATP. The dephosphorylation reaction was terminated by acid quenching after the indicated time intervals. A bi-exponential decay function was fitted to the data. The rate constant corresponding to the rapid phase, reflecting the ADP reaction with E_1P, was set to 2 s^{-1}. The fraction of E_1P phosphoenzyme obtained from this analysis is indicated in the panel (also listed in Table 2 with statistics). The wild type data are represented in each panel by a *dotted line*.

display a reduced catalytic turnover rate relative to wild type. A reduced turnover rate has previously been reported for mutants T263M, T345A, M731T, and R834Q, but the responsible change(s) were not elucidated (4, 9, 10). Our rapid kinetic studies of the phosphorylation from ATP identify a reduced V_{max} of phosphorylation as a major factor contributing to the reduction of the catalytic turnover rate of mutants V138A, T345A, R593W, V628M, M731T, and R834Q. These mutants displayed decreases in the V_{max} of phosphorylation of 2–6-fold (Fig. 6 and Table 2). To be able to carry out transient kinetic measurements, oligomycin was added to promote phosphorylation by stabilizing the Na^+-occluded $E_1[Na_3]$ form and blocking the $E_1P[Na_3] \rightarrow E_2P$ transition. In the absence of oligomycin, the relative level of phosphoenzyme at steady state was in fact very low for R593W, V628M, M731T, and R834Q (Table 2, "EP/EP_{oligo}"), suggesting that under physiological conditions without oligomycin the phosphorylation rate is even more dramatically affected than judged from the kinetic data obtained with oligomycin.

The low phosphorylation rate also accounts for the enhanced K^+ inhibition of ATPase activity at high K^+ concentrations seen particularly for R593W, V628M, M731T, and R834Q (Fig. 2). Hence, the low phosphorylation rate leads to increased availability of E_1 at steady state and consequently to enhanced K^+ competition with Na^+ at the intracellular E_1 sites. In the living cell with cytoplasmic concentrations of ~150 mM K^+ and only ~10 mM Na^+, the enhanced K^+ competition with Na^+ may be highly relevant as a factor contributing to compromise pump function.

For R593W, V628M, E700K, M731T, and R834Q, the apparent affinity for vanadate was lowered to an extent that could not be accounted for by the observed shift of the conformational equilibrium toward E_1 (Fig. 8 and Table 1). Because vanadate binds at the phosphorylation site of the E_2 form as an analog of the phosphoryl group in the transition state between E_2 and E_2P, the extraordinary low affinity for vanadate might be related to a perturbation of the phosphorylation site in E_2 and/or the transition state. For the mutants showing both a reduced V_{max} of phosphorylation from ATP in E_1 and an extraordinary low affinity for vanadate (R593W, V628M, M731T, and R834Q), the underlying structural changes in E_1 and E_2 forms might be similar. By contrast E700K did not show a reduced phosphorylation rate with ATP, and for this mutant the phosphorylation site therefore seems not to be perturbed in E_1. Besides its extraordinary lack of sensitivity to vanadate, E700K was characterized by a relatively low maximal rate of dephosphorylation of E_2P (42 s^{-1} *versus* 132 s^{-1} for wild type), which probably causes the reduced catalytic turnover rate of E700K. Both the disruption of vanadate binding and the reduced dephosphorylation rate can be explained by assuming that the transition state of E_2P dephosphorylation is destabilized. It is furthermore of note that E700K exhibited an increased apparent affinity for ouabain, and even though E700K did not show reduced affinity for K^+ activation of dephosphorylation (Fig. 3 and Table 2), a slight 1.6-fold reduction of apparent K^+ affinity in activation of ATPase activity was noted (Fig. 2 and Table 1). Both of these effects might result from accumulation at steady state of the $E_2P[Na_2]$ phosphoenzyme form, which is an intermediate in the $E_1P[Na_3] \rightarrow E_2P$ transition (31) exhibiting a particularly high affinity for cardiotonic steroids ("E*P" *cf.* Refs 32 and 33). Thus, the evidence indicates that mutation E700K is most disturbing in the part of the pump cycle involving E_2P and E_2P-like states.

From the crystal structure it is known how the residues studied here are positioned in the $E_2[K_2]$ state with bound MgF_4^{2-} as a phosphate analog (18, 19), and although crystal structures are static snapshots without the flexibility of the native enzyme, they are useful as a basis for analysis of the mechanisms under-

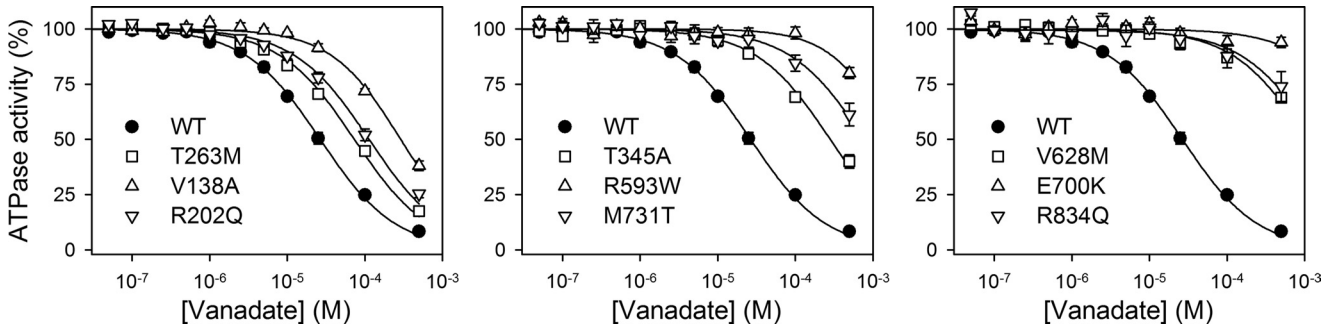

FIGURE 8. **Vanadate dependence of Na^+,K^+-ATPase activity.** ATPase activity was measured at 37 °C in 130 mM NaCl, 20 mM KCl, 3 mM $MgCl_2$, 3 mM ATP, 30 mM histidine (pH 7.4), 1 mM EGTA, 10 μM ouabain, and vanadate concentrations as indicated. Each *line* represents the best fit of the equation $V = V_{max}\cdot(1 - [\text{vanadate}]^n/(K_{0.5}{}^n + [\text{vanadate}]^n))$, with n ranging between 0.9 and 1.1, giving the $K_{0.5}$ values indicated in Table 1.

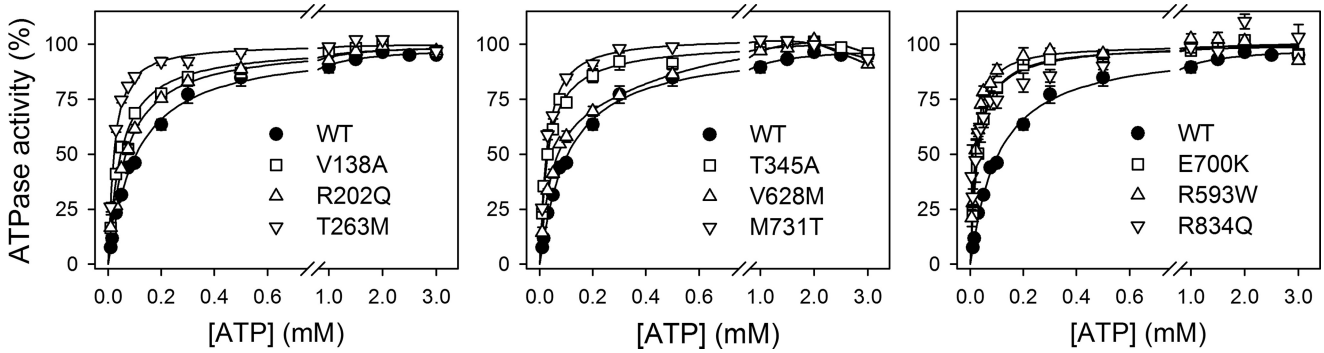

FIGURE 9. **ATP dependence of Na^+,K^+-ATPase activity.** ATPase activity was measured at 37 °C in the presence of 130 mM NaCl, 20 mM KCl, 3 mM $MgCl_2$, 30 mM histidine (pH 7.4), 1 mM EGTA, 10 μM ouabain, and the indicated concentrations of ATP. $K_{0.5}$ values for activation are listed in Table 1.

lying the observed mutational effects. Arg^{593}, Val^{628}, Glu^{700}, and Met^{731} are located in the Rossmann fold, which is a central feature of the P-domain, consisting of a seven-stranded parallel β-sheet associated with seven short α-helices (P1–P7) as indicated in Fig. 10. Asp^{374} (phosphorylation site) and residues involved in Mg^{2+} binding, Thr^{376}, Asp^{714}, and Asp^{718}, are located centrally in the Rossmann fold (Fig. 10). The phosphorylation of Asp^{374} is triggered by an approach between the N- and P-domains associated with a bending of the P-domain. This conformational change is the result of transmission of the effect of Mg^{2+} binding to the P7 helix of the Rossmann fold (34, 35), meaning that the loop between β6 and P7, where Met^{731} is located (Figs. 10 and 11), has to be strained when Mg^{2+} binds to Asp^{714}. The role of Met^{731} may thus be to reduce the freedom of movement of this loop, thereby ensuring the strain. In fact the side chain of Met^{731} is flanked on one side by Asp^{714}, Thr^{378}, and Arg^{593} (Fig. 10*B*), and the introduction of the threonine side chain in M731T likely pushes Asp^{714}, thus preventing a proper bending of the P-domain. It is interesting to note that M731T and R593W are the mutations giving the largest reduction of phosphorylation rate observed in this study (*cf.* Table 2). Considering that the Met^{731} and Arg^{593} side chains are located within a distance of only 4–5 Å from each other in the crystal structure (Fig. 10, *A* and *B*), it is possible that the bulky tryptophan in R593W actually interferes by disturbing Met^{731}. Furthermore, Arg^{593} is within hydrogen bonding distance of the backbone carbonyls of Gly^{377} and Thr^{378}, which are located in the same loop as Asp^{374} and Thr^{376} (Fig. 10, *A* and *B*). The clash resulting from insertion of the tryptophan might therefore also disturb phosphorylation by shifting the positions of Asp^{374} and Thr^{376}. It is noteworthy that mutations T376M and T378N have been found in familial hemiplegic migraine patients and were reported as loss of function mutations based on cell survival studies (14, 36–38).

The valine replaced in mutant V628M is positioned at the end of the P3 helix in the Rossmann fold. It is part of a hydrophobic/van der Waals interaction network (Fig. 10, *A* and *C*), and the interaction with Pro^{592} and Val^{596} at the N-terminal end of the P2 helix may contribute to stabilize the positions of helices P2 and P3. The V628M mutation might lead to a shift of the position of Pro^{592}, thereby disturbing the interactions of the adjacent Arg^{593} with Gly^{377} and Thr^{378} mentioned above.

The glutamate replaced in E700K is located in the P5 helix of the Rossmann fold. In the crystal structure of the Na^+,K^+-ATPase $E_2[K_2]$ state with bound MgF_4^{2-}, Glu^{700} is positioned between two positively charged residues, Arg^{704} (at the end of the P5 helix) and Lys^{724} (P6 helix), with a distance of 4.6 Å to each (Fig. 10*A*). Moreover, Lys^{724} is within hydrogen bonding distance to Gln^{703} in the P5 helix (2.7 Å). It can be imagined that the extra positive charge introduced between Arg^{704} and Lys^{724} by E700K leads to a repulsion between the three positive charges disturbing the positioning of P5 and P6. Such a disturbance could lead to a shift of β5 and the loop between β5 and P6 containing Asp^{714} and Asp^{718} critical to Mg^{2+} binding (Fig. 10*A*). We wondered whether Glu^{700} and either Lys^{724} or Arg^{704} might actually be closer to each other in the vanadate-bound E_2 state than the 4.6 Å in the $E_2[K_2]$ crystal structure. The Na^+,K^+-ATPase residues Glu^{700}, Lys^{724}, and Gln^{703} are conserved as Glu^{689}, Lys^{713}, and Gln^{692} in the Ca^{2+}-ATPase, which has been crystallized not only in the MgF_4^{2-}-bound E_2 form

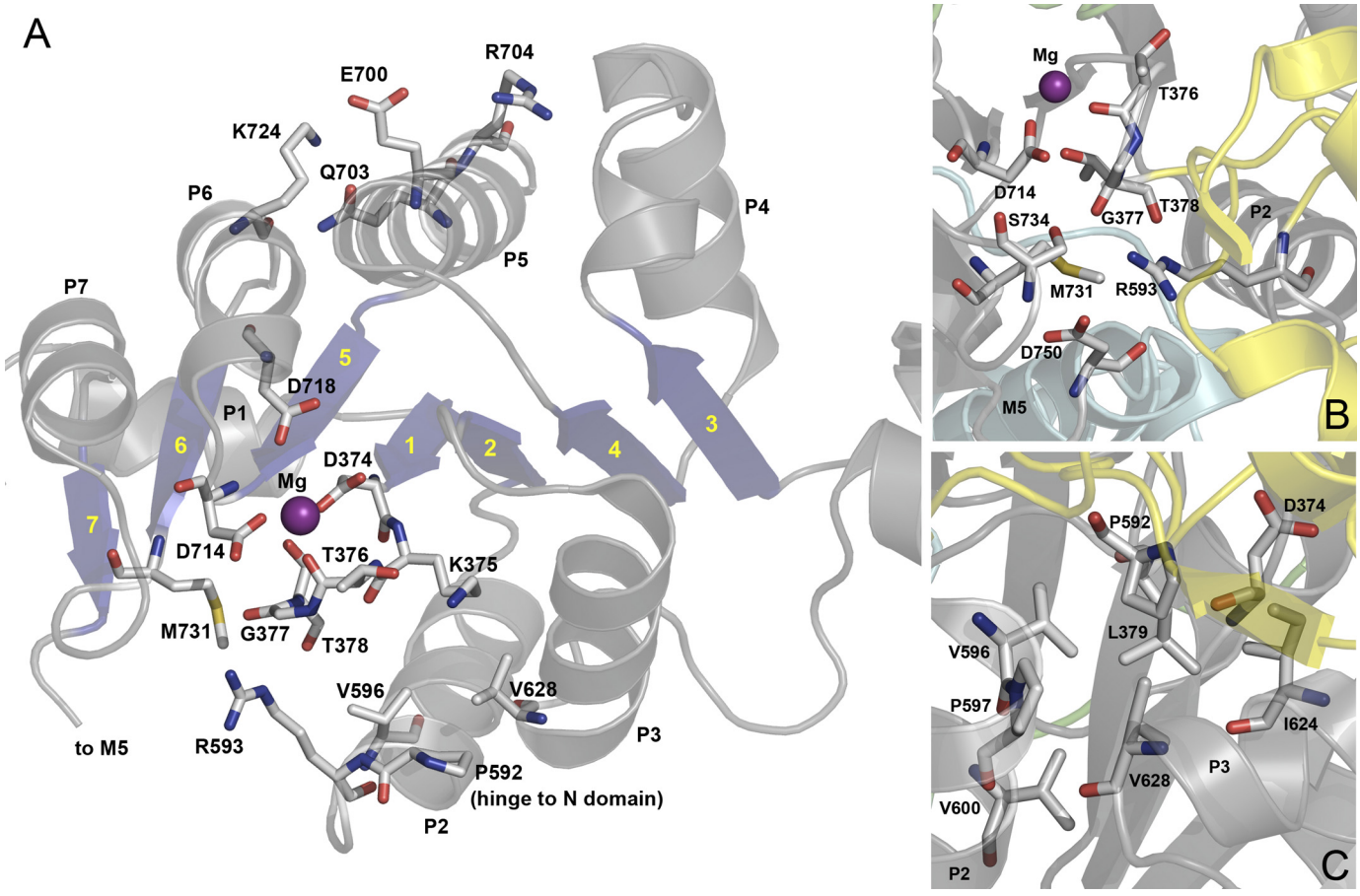

FIGURE 10. **Location of the FHM2 mutations with relation to the Rossmann fold in the Na^+,K^+-ATPase structure.** The structure used is the same as in Fig. 1. Side chains corresponding to mutated residues and interaction partners (numbered according to the human α2-isoform) are highlighted as *sticks*, as are key residues in the catalytic site as follows: Thr^{376}, Asp^{714}, and Asp^{718} (Mg^{2+}-binding residues), and Asp^{374} (phosphorylation site). Atoms are colored according to the elements (carbon, *gray*; oxygen, *red*; nitrogen, *blue*; sulfur, *yellow*). The catalytic Mg^{2+} ion is shown as a *purple sphere*. *A,* Rossmann fold of the P-domain viewed from the cytosol. *P1–P7* helices with interposed β-strands (*blue arrows* with *yellow numbers 1–7*) are indicated. Note the proximity of Arg^{593} and Met^{731} to Gly^{377} and Thr^{378}, and the position of Glu^{700} between the two positively charged side chains of Arg^{704} and Lys^{724}. *B,* close up of interaction network around Arg^{593} and Met^{731}. *C,* close up of hydrophobic/van der Waals interaction network around Val^{628} (Pro^{592} and Val^{596} also indicated in *A*).

similar to the Na^+,K^+-ATPase crystal form but also in several other E_2 states, including the AlF_4^--bound form. The latter is considered the state closest to the E_2 form with vanadate bound, as AlF_4^- and vanadate are both believed to mimic the trigonal bipyramidal structure of the penta-coordinated phosphate in the transition state of E_2P dephosphorylation (39, 40). Interestingly, among the AlF_4^--bound E_2 crystal structures of the Ca^{2+}-ATPase, 4 out of 7 have a distance between Glu^{689} and Lys^{713} <4 Å, *i.e.* short enough to indicate the presence of a salt link between these residues in the E_2P transition state. In contrast, in the MgF_4^{2-}-bound Ca^{2+}-ATPase structures, the corresponding distance is 4–5 Å, consistent with the distance in the MgF_4^{2-}-bound form of Na^+,K^+-ATPase (*cf.* supplemental Table S1). If this scenario for the E_2P transition state were extrapolated to the Na^+,K^+-ATPase, it would explain the very strong destabilization of the vanadate-bound state of E700K (Fig. 8). If in addition Glu^{700} and Lys^{724} were further apart in the $E_1[Na_3]$ state, the lack of effect of the mutation on the phosphorylation from ATP would be understandable. The Ca^{2+}-ATPase E_1 structures do not provide a clear answer to this question, but it is noteworthy that 4 out of 8 E_1 structures show a distance larger than 4 Å (*cf.* supplemental Table S1).

T345A in the cytoplasmic extension of M4 and R834Q in the L6–7 loop are both located at the boundary between the P-domain and the transmembrane region, and the reason that these mutations also reduce the phosphorylation rate significantly may be the participation of Thr^{345} and Arg^{834} in interaction networks involving helices connected with the Rossmann fold (Fig. 11). Thr^{345} might participate in van der Waals interactions with Val^{362} at the N-terminal end of the P-domain helix P1, from which the central β-strand of the Rossmann fold (β-strand "1" in Fig. 11) leads to the phosphorylation site with Asp^{374}. Interestingly, mutation V362E has also been found in patients with FHM2 (41). Depending on the actual rotational state of the Thr^{345} side chain, the hydroxyl group might form a hydrogen bond with Glu^{761} of M5. Mutation R834Q seems to disrupt bonds from P1-helix residues Glu^{363} and Ser^{367} (C-terminal end of the P1-helix) to the L6–7 loop (19). R834Q furthermore disrupts the bond between Arg^{834} and Glu^{285} of M3 (Fig. 11), which may explain the reduction of Na^+ affinity caused by R834Q, since mutation of Glu^{285} has been shown to reduce Na^+ affinity, possibly a consequence of the involvement of Glu^{285} in control of the cytoplasmic entrance pathway for Na^+ (22).

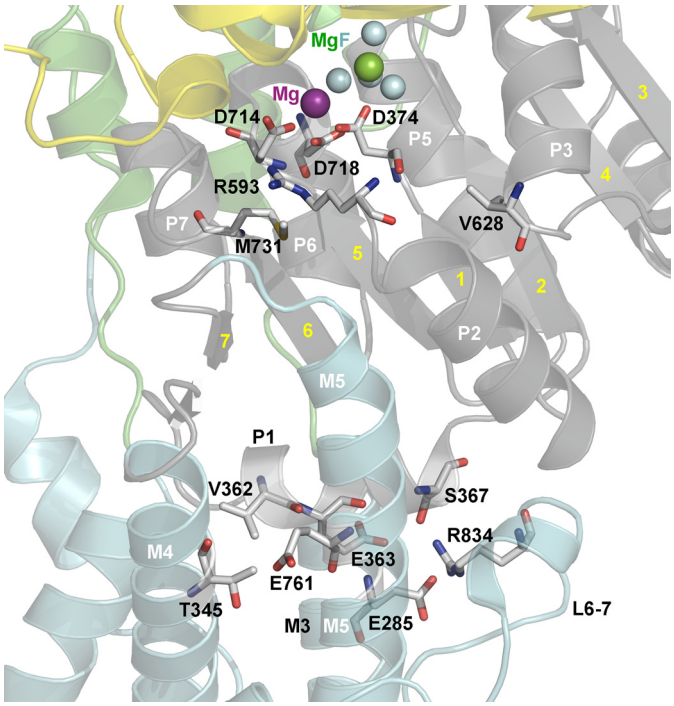

FIGURE 11. **Side view of the membrane interface of the P-domain.** The structure used is the same as in Fig. 1 with the same color codes for P-, A-, N-, and M-domain, and the phosphate analog MgF_4^{2-} (*MgF*) shown as *one green* and *four cyan spheres*. Side chains corresponding to mutated residues and interaction partners (numbered according to the human α2-isoform) are highlighted as *sticks*, as are key residues in the catalytic site. Atoms are colored according to the elements (carbon, *gray*; oxygen, *red*; nitrogen, *blue*; sulfur, *yellow*). P-domain helices *P1–P3* and *P5–P7* as well as the interposed β-strands (*yellow numbers*) and transmembrane helices *M3–M5* are indicated. Note the location of the P1 helix with Val^{362} interacting with Thr^{345}, and Glu^{363} and Ser^{367} interacting with Arg^{834}. Glu^{761} (*M5*) may also interact with Thr^{345}, depending on the actual rotational state of Thr^{345}. In addition, Glu^{285} (*M3*) interacts with Arg^{834}.

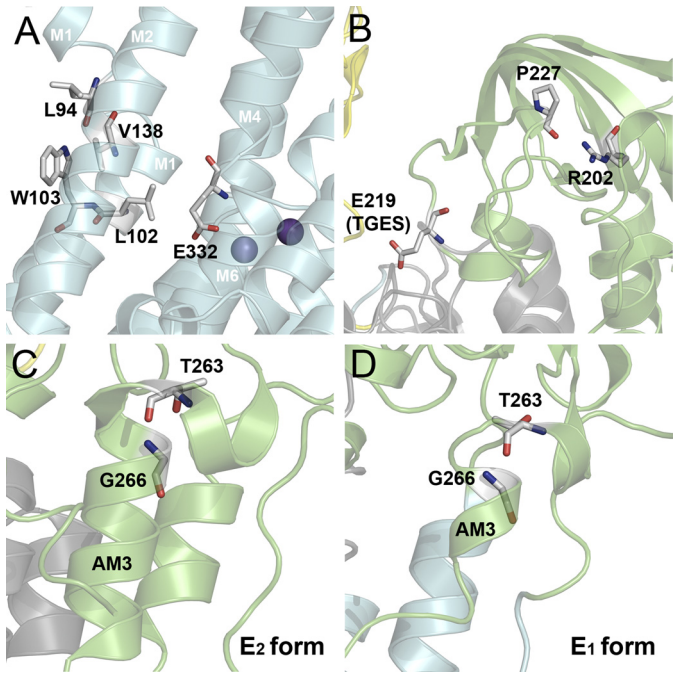

FIGURE 12. **Structural relationships of residues altered in mutants V138A, R202Q, and T263M.** The structure used in *A–C* is the same as in Fig. 1 with the same color codes for P-, A-, N-, and M-domain. Side chains corresponding to mutated residues and interaction partners (numbered according to the human α2-isoform) are highlighted as *sticks*. Atoms are colored according to the elements (carbon, *gray*; oxygen, *red*; nitrogen, *blue*). *A*, Val^{138} in M2 interacts with M1 residues Leu^{94} and Trp^{103}. *B*, interaction between Arg^{202} and Pro^{227} may stabilize the loop containing the conserved TGES motif with Glu^{219}. *C*, Thr^{263} is located in the AM3 linker segment connecting the A-domain to the M3 transmembrane segment (*cf.* Fig. 1). In the E_2 and E_2P conformations, part of the AM3 linker is coiled up, forming an α-helical arrangement, which is partially unwound at Thr^{263}, with the two parts of the α-helix being almost orthogonal to each other. The side chain hydroxyl group of the threonine is within hydrogen bonding distance to the backbone amide nitrogen of Gly^{266}. *D*, homology model of the Na^+,K^+-ATPase in E_1 based on the structure of the closely related Ca^{2+}-ATPase in E_1 (Protein Data Bank code 1T5T). The helical structure of the AM3 linker is much more unwound than in E_2 conformations of Na^+,K^+-ATPase and Ca^{2+}-ATPase, with less strict requirement for the bond between Thr^{263} and Gly^{266}.

Surprisingly, the mutation V138A also had significant impact on the phosphorylation rate, even though Val^{138} is positioned in the transmembrane segment M2 far from the phosphorylation site, thus indicating a long range effect, which might be exerted through interference with the hydrophobic/van der Waals interactions between M1 and M2 (*cf.* Fig. 12*A*). These interactions seem to allow M1 to close the Na^+ binding pocket through contact with the ion binding Glu^{332} of M4 (42), a conformational change believed to be propagated to the phosphorylation site in a yet undefined way and result in phosphoryl transfer (35). Indeed, a reduced rate of phosphorylation was previously observed following replacement of M1 residues Leu^{94} and Gly^{97} (42, 43).

For R202Q and T263M, the phosphorylation rate was wild type-like, and the reason for the reduced catalytic turnover rate seems to be a slow conversion of E_1P to E_2P, in particular T263M showed a conspicuous accumulation of E_1P. Furthermore, both R202Q and T263M appeared to shift the E_1-E_2 distribution of the dephosphoenzyme in favor of E_1. These mutations are both associated with the A-domain, which undergoes drastic structural rearrangements during the E_1-E_2 and E_1P-E_2P transitions (35, 44). Arg^{202} is positioned in a β-strand of the A-domain, where it appears to form a hydrogen bond with the backbone carbonyl oxygen of Pro^{227} (2.7 Å distance, Fig. 12*B*). This bond could be important for stabilization of the loop containing the conserved TGES motif, and hence for interaction of TGES with the P-domain in E_2 and E_2P. Thr^{263} is located in the AM3 linker segment connecting the A-domain to M3 and appears to be involved in stabilization of the kinked α-helix present in the AM3 linker in E_2, but not in E_1 (see Fig. 12, *C* and *D*). Hence, in E_2 the side chain hydroxyl group of the threonine seems to form a hydrogen bond with the backbone amide nitrogen of Gly^{266} (2.8 Å distance). This structural arrangement is likely destabilized by the T263M substitution due to the bulkiness of the methionine side chain. The ability of the E_1 conformation to better accommodate the methionine, due to a looser structure compared with the helical arrangement in E_2 (Fig. 12*D*), explains that the conformational equilibrium is shifted toward E_1 in the mutant. In line with this interpretation, mutation of Gly^{266} to alanine, disturbing the kinked helix arrangement, was previously shown to cause accumulation of E_1 (45).

To summarize, if disturbance of K^+ clearance by glial cells is the reason for development of FHM2, this disturbance must be attributed to a low maximum turnover rate of the Na^+,K^+-ATPase and not to a reduced affinity for external K^+. In several of the FHM2 mutants studied here, the function of the catalytic

site in phosphorylation (V138A, T345A, R593W, V628M, M731T, and R834Q) or dephosphorylation (E700K) is affected, involving local effects on the catalytic assembly as well as helices connected with the Rossmann fold, and long range effects transmitted from as far away as the membrane domain. The last two mutations (R202Q and T263M) affect the maximum turnover rate by destabilizing the A-domain in the E_2/E_2P conformations.

Acknowledgments—We thank Kirsten Lykke Pedersen, Janne Petersen, and Nina Juste for expert technical assistance. We also thank Professor C. Toyoshima, University of Tokyo, for discussion and helpful suggestions.

REFERENCES

1. De Fusco, M., Marconi, R., Silvestri, L., Atorino, L., Rampoldi, L., Morgante, L., Ballabio, A., Aridon, P., and Casari, G. (2003) Haploinsufficiency of ATP1A2 encoding the Na^+/K^+ pump $\alpha2$ subunit associated with familial hemiplegic migraine type 2. *Nat. Genet.* **33,** 192–196
2. McGrail, K. M., Phillips, J. M., and Sweadner, K. J. (1991) Immunofluorescent localization of three Na,K-ATPase isozymes in the rat central nervous system: both neurons and glia can express more than one Na,K-ATPase. *J. Neurosci.* **11,** 381–391
3. Somjen, G. G. (2001) Mechanisms of spreading depression and hypoxic spreading depression-like depolarization. *Physiol. Rev.* **81,** 1065–1096
4. Segall, L., Scanzano, R., Kaunisto, M. A., Wessman, M., Palotie, A., Gargus, J. J., and Blostein, R. (2004) Kinetic alterations due to a missense mutation in the Na,K-ATPase $\alpha2$ subunit cause familial hemiplegic migraine type 2. *J. Biol. Chem.* **279,** 43692–43696
5. Lencesova, L., O'Neill, A., Resneck, W. G., Bloch, R. J., and Blaustein, M. P. (2004) Plasma membrane-cytoskeleton-endoplasmic reticulum complexes in neurons and astrocytes. *J. Biol. Chem.* **279,** 2885–2893
6. Rose, E. M., Koo, J. C., Antflick, J. E., Ahmed, S. M., Angers, S., and Hampson, D. R. (2009) Glutamate transporter coupling to Na,K-ATPase. *J. Neurosci.* **29,** 8143–8155
7. Jen, J. C., Klein, A., Boltshauser, E., Cartwright, M. S., Roach, E. S., Mamsa, H., and Baloh, R. W. (2007) Prolonged hemiplegic episodes in children due to mutations in ATP1A2. *J. Neurol. Neurosurg. Psychiatry* **78,** 523–526
8. Todt, U., Dichgans, M., Jurkat-Rott, K., Heinze, A., Zifarelli, G., Koenderink, J. B., Goebel, I., Zumbroich, V., Stiller, A., Ramirez, A., Friedrich, T., Göbel, H., and Kubisch, C. (2005) Rare missense variants in ATP1A2 in families with clustering of common forms of migraine. *Hum. Mutat.* **26,** 315–321
9. Segall, L., Mezzetti, A., Scanzano, R., Gargus, J. J., Purisima, E., and Blostein, R. (2005) Alterations in the $\alpha2$ isoform of Na,K-ATPase associated with familial hemiplegic migraine type 2. *Proc. Natl. Acad. Sci. U.S.A.* **102,** 11106–11111
10. Tavraz, N. N., Friedrich, T., Dürr, K. L., Koenderink, J. B., Bamberg, E., Freilinger, T., and Dichgans, M. (2008) Diverse functional consequences of mutations in the Na^+/K^+-ATPase $\alpha2$-subunit causing familial hemiplegic migraine type 2. *J. Biol. Chem.* **283,** 31097–31106
11. Vanmolkot, K. R., Stam, A. H., Raman, A., Koenderink, J. B., de Vries, B., van den Boogerd, E. H., van Vark, J., van den Heuvel, J. J., Bajaj, N., Terwindt, G. M., Haan, J., Frants, R. R., Ferrari, M. D., and van den Maagdenberg, A. M. (2007) First case of compound heterozygosity in Na,K-ATPase gene ATP1A2 in familial hemiplegic migraine. *Eur. J. Hum. Genet.* **15,** 884–888
12. Vanmolkot, K. R., Kors, E. E., Hottenga, J. J., Terwindt, G. M., Haan, J., Hoefnagels, W. A., Black, D. F., Sandkuijl, L. A., Frants, R. R., Ferrari, M. D., and van den Maagdenberg, A. M. (2003) Novel mutations in the Na^+, K^+-ATPase pump gene ATP1A2 associated with familial hemiplegic migraine and benign familial infantile convulsions. *Ann. Neurol.* **54,** 360–366
13. Kaunisto, M. A., Harno, H., Vanmolkot, K. R., Gargus, J. J., Sun, G., Hämäläinen, E., Liukkonen, E., Kallela, M., van den Maagdenberg, A. M., Frants, R. R., Färkkilä, M., Palotie, A., and Wessman, M. (2004) A novel missense ATP1A2 mutation in a Finnish family with familial hemiplegic migraine type 2. *Neurogenetics* **5,** 141–146
14. Riant, F., De Fusco, M., Aridon, P., Ducros, A., Ploton, C., Marchelli, F., Maciazek, J., Bousser, M. G., Casari, G., and Tournier-Lasserve, E. (2005) ATP1A2 mutations in 11 families with familial hemiplegic migraine. *Hum. Mutat.* **26,** 281
15. Pierelli, F., Grieco, G. S., Pauri, F., Pirro, C., Fiermonte, G., Ambrosini, A., Costa, A., Buzzi, M. G., Valoppi, M., Caltagirone, C., Nappi, G., and Santorelli, F. M. (2006) A novel ATP1A2 mutation in a family with FHM type II. *Cephalalgia* **26,** 324–328
16. Vanmolkot, K. R., Kors, E. E., Turk, U., Turkdogan, D., Keyser, A., Broos, L. A., Kia, S. K., van den Heuvel, J. J., Black, D. F., Haan, J., Frants, R. R., Barone, V., Ferrari, M. D., Casari, G., Koenderink, J. B., and van den Maagdenberg, A. M. (2006) Two *de novo* mutations in the Na,K-ATPase gene ATP1A2 associated with pure familial hemiplegic migraine. *Eur. J. Hum. Genet.* **14,** 555–560
17. Thomsen, L. L., Kirchmann, M., Bjornsson, A., Stefansson, H., Jensen, R. M., Fasquel, A. C., Petursson, H., Stefansson, M., Frigge, M. L., Kong, A., Gulcher, J., Stefansson, K., and Olesen, J. (2007) The genetic spectrum of a population-based sample of familial hemiplegic migraine. *Brain* **130,** 346–356
18. Morth, J. P., Pedersen, B. P., Toustrup-Jensen, M. S., Sørensen, T. L., Petersen, J., Andersen, J. P., Vilsen, B., and Nissen, P. (2007) Crystal structure of the sodium-potassium pump. *Nature* **450,** 1043–1049
19. Shinoda, T., Ogawa, H., Cornelius, F., and Toyoshima, C. (2009) Crystal structure of the sodium-potassium pump at 2.4 A resolution. *Nature* **459,** 446–450
20. Vilsen, B. (1992) Functional consequences of alterations to Pro-328 and Leu-332 located in the 4th transmembrane segment of the α-subunit of the rat kidney Na^+,K^+-ATPase. *FEBS Lett.* **314,** 301–307
21. Rodacker, V., Toustrup-Jensen, M., and Vilsen, B. (2006) Mutations Phe785Leu and Thr618Met in Na^+,K^+-ATPase, associated with familial rapid-onset dystonia parkinsonism, interfere with Na^+ interaction by distinct mechanisms. *J. Biol. Chem.* **281,** 18539–18548
22. Toustrup-Jensen, M., and Vilsen, B. (2002) Importance of Glu(282) in transmembrane segment M3 of the Na^+,K^+-ATPase for control of cation interaction and conformational changes. *J. Biol. Chem.* **277,** 38607–38617
23. Skou, J. C. (1957) The influence of some cations on an adenosine triphosphatase from peripheral nerves. *Biochim. Biophys. Acta* **23,** 394–401
24. Vilsen, B. (1999) Mutant Phe788 → Leu of the Na^+,K^+-ATPase is inhibited by micromolar concentrations of potassium and exhibits high Na^+-ATPase activity at low sodium concentrations. *Biochemistry* **38,** 11389–11400
25. Esmann, M., and Skou, J. C. (1985) Occlusion of Na^+ by the Na,K-ATPase in the presence of oligomycin. *Biochem. Biophys. Res. Commun.* **127,** 857–863
26. Skou, J. C. (1991) in *The Sodium Pump: Recent Developments* (Kaplan, J. H., and De Weer, P., eds) pp. 317–319, The Rockefeller University Press, New York
27. Fedosova, N. U., Champeil, P., and Esmann, M. (2003) Rapid filtration analysis of nucleotide binding to Na,K-ATPase. *Biochemistry* **42,** 3536–3543
28. Cantley, L. C., Jr., Cantley, L. G., and Josephson, L. (1978) A characterization of vanadate interactions with the Na,K-ATPase. Mechanistic and regulatory implications. *J. Biol. Chem.* **253,** 7361–7368
29. Blanco-Arias, P., Einholm, A. P., Mamsa, H., Concheiro, C., Gutiérrez-de-Terán, H., Romero, J., Toustrup-Jensen, M. S., Carracedo, A., Jen, J. C., Vilsen, B., and Sobrido, M. J. (2009) A C-terminal mutation of ATP1A3 underscores the crucial role of sodium affinity in the pathophysiology of rapid-onset dystonia-parkinsonism. *Hum. Mol. Genet.* **18,** 2370–2377
30. Einholm, A. P., Toustrup-Jensen, M. S., Holm, R., Andersen, J. P., and Vilsen, B. (2010) The rapid-onset dystonia parkinsonism mutation D923N of the Na^+,K^+-ATPase $\alpha3$ isoform disrupts Na^+ interaction at the third Na^+ site. *J. Biol. Chem.* **285,** 26245–26254
31. Jorgensen, P. L. (1991) in *The Sodium Pump: Structure, Mechanism, and Regulation* (Kaplan, J. H., and De Weer, P., eds) pp. 189–200, The Rockefeller University Press, New York

32. Yoda, A., and Yoda, S. (1987) Two different phosphorylation-dephosphorylation cycles of Na,K-ATPase proteoliposomes accompanying Na^+ transport in the absence of K^+. *J. Biol. Chem.* **262,** 110–115
33. Yoda, S., and Yoda, A. (1987) Phosphorylated intermediates of Na,K-ATPase proteoliposomes controlled by bilayer cholesterol. Interaction with cardiac steroid. *J. Biol. Chem.* **262,** 103–109
34. Toyoshima, C., and Mizutani, T. (2004) Crystal structure of the calcium pump with a bound ATP analogue. *Nature* **430,** 529–535
35. Toyoshima, C. (2009) How Ca^{2+}-ATPase pumps ions across the sarcoplasmic reticulum membrane. *Biochim. Biophys. Acta* **1793,** 941–946
36. Castro, M. J., Stam, A. H., Lemos, C., Barros, J., Gouveia, R. G., Martins, I. P., Koenderink, J. B., Vanmolkot, K. R., Mendes, A. P., Frants, R. R., Ferrari, M. D., Sequeiros, J., Pereira-Monteiro, J. M., and van den Maagdenberg, A. M. (2007) Recurrent ATP1A2 mutations in Portuguese families with familial hemiplegic migraine. *J. Hum. Genet.* **52,** 990–998
37. Bassi, M. T., Bresolin, N., Tonelli, A., Nazos, K., Crippa, F., Baschirotto, C., Zucca, C., Bersano, A., Dolcetta, D., Boneschi, F. M., Barone, V., and Casari, G. (2004) A novel mutation in the ATP1A2 gene causes alternating hemiplegia of childhood. *J. Med. Genet.* **41,** 621–628
38. Swoboda, K. J., Kanavakis, E., Xaidara, A., Johnson, J. E., Leppert, M. F., Schlesinger-Massart, M. B., Ptacek, L. J., Silver, K., and Youroukos, S. (2004) Alternating hemiplegia of childhood or familial hemiplegic migraine? A novel ATP1A2 mutation. *Ann. Neurol.* **55,** 884–887
39. Danko, S., Yamasaki, K., Daiho, T., and Suzuki, H. (2004) Distinct natures of beryllium fluoride-bound, aluminum fluoride-bound, and magnesium fluoride-bound stable analogues of an ADP-insensitive phosphoenzyme intermediate of sarcoplasmic reticulum Ca^{2+}-ATPase: changes in catalytic and transport sites during phosphoenzyme hydrolysis. *J. Biol. Chem.* **279,** 14991–14998
40. Cornelius, F., Mahmmoud, Y. A., and Toyoshima, C. (2011) Metal fluoride complexes of Na,K-ATPase: characterization of fluoride-stabilized phosphoenzyme analogues and their interaction with cardiotonic steroids. *J. Biol. Chem.* **286,** 29882–29892
41. Castro, M. J., Nunes, B., de Vries, B., Lemos, C., Vanmolkot, K. R., van den Heuvel, J. J., Temudo, T., Barros, J., Sequeiros, J., Frants, R. R., Koenderink, J. B., Pereira-Monteiro, J. M., and van den Maagdenberg, A. M. (2008) Two novel functional mutations in the Na^+,K^+-ATPase α2-subunit ATP1A2 gene in patients with familial hemiplegic migraine and associated neurological phenotypes. *Clin. Genet.* **73,** 37–43
42. Einholm, A. P., Andersen, J. P., and Vilsen, B. (2007) Importance of Leu99 in transmembrane segment M1 of the Na^+, K^+-ATPase in the binding and occlusion of K^+. *J. Biol. Chem.* **282,** 23854–23866
43. Einholm, A. P., Toustrup-Jensen M., Andersen, J. P., and Vilsen, B. (2005) Mutation of Gly-94 in transmembrane segment M1 of Na^+,K^+-ATPase interferes with Na^+ and K^+ binding in E2P conformation. *Proc. Natl. Acad. Sci. U.S.A.* **102,** 11254–11259
44. Patchornik, G., Goldshleger, R., and Karlish, S. J. (2000) The complex ATP-Fe^{2+} serves as a specific affinity cleavage reagent in ATP-Mg^{2+} sites of Na,K-ATPase: altered ligation of Fe^{2+} Mg^{2+} ions accompanies the E1 $\rightarrow$ E2 conformational change. *Proc. Natl. Acad. Sci. U.S.A.* **97,** 11954–11959
45. Toustrup-Jensen, M., Hauge, M., and Vilsen, B. (2001) Mutational effects on conformational changes of the dephospho- and phospho-forms of the Na^+,K^+-ATPase. *Biochemistry* **40,** 5521–5532